coatings

Article

Optical Interference Filters Combined with Thin Film Residual Stress Compensation for Image Contrast Enhancement

Chuen-Lin Tien [1,2,*], Shu-Hui Su [2], Ching-Ying Cheng [3], Yuan-Ming Chang [2] and Dong-Han Mo [2]

1 Department of Electrical Engineering, Feng Chia University, Taichung 40724, Taiwan
2 *Ph.D.* Program in Electrical and Communications Engineering, Feng Chia University, Taichung 40724, Taiwan; su4182003@yahoo.com.tw (S.-H.S.); mason.jyishing@gmail.com (Y.-M.C.); p1000459@o365.fcu.edu.tw (D.-H.M.)
3 Department of Optometry, Chung Shan Medical University, Taichung 402, Taiwan
* Correspondence: cltien@fcu.edu.tw

Abstract: We propose two single-wavelength notch filters and one dual-wavelength (480 and 620 nm) notch filter to enhance image contrast. The stack structure of the notch filters was designed as $(Ta_2O_5/SiO_2)^4Ta_2O_5$ in Essential Macleod thin film simulation software. Dual-electron-beam evaporation with ion beam-assisted deposition was used to prepare optical interference filters with different center wavelengths. A multilayer notch filter with a center wavelength of 620 nm was deposited on the front surface of the glass, and then a notch filter with a center wavelength of 480 nm was coated on the rear surface of the same glass. The proposed dual-wavelength (480 and 620 nm) notch filter is a combination of two single-wavelength notch filters coated on a double-sided glass substrate to compensate for residual stress. The transmittance, residual stress, and surface roughness of the proposed notch filter were evaluated using different measuring instruments. The experimental results show that the residual stress of the dual-wavelength notch filter could be reduced to 10.8 MPa by using a double-sided coating technique. The root-mean-square (RMS) surface roughness of the notch filters was measured by using a Linnik microscopic interferometer. The RMS surface roughness was 1.80 for the 620 nm notch filter and 2.09 for the 480 nm notch filter. The image contrast obtained with the three different notch filters was measured using an optical microscope and a CMOS camera. The contrast value could be increased from 0.328 (without a filter) to 0.696 (dual-wavelength notch filter).

Keywords: optical interference filter; notch filter; electron beam evaporation; ion beam-assisted deposition; residual stress; surface roughness

Citation: Tien, C.-L.; Su, S.-H.; Cheng, C.-Y.; Chang, Y.-M.; Mo, D.-H. Optical Interference Filters Combined with Thin Film Residual Stress Compensation for Image Contrast Enhancement. *Coatings* **2023**, *13*, 857. https://doi.org/10.3390/coatings13050857

Academic Editor: Mihai Anastasescu

Received: 6 April 2023
Revised: 25 April 2023
Accepted: 28 April 2023
Published: 30 April 2023

1. Introduction

Choosing the correct optical interference filter can improve the contrast of captured images and reduce the processing time required to extract relevant image data. Contrast is defined as the difference in light intensity between an image and an adjacent background relative to the overall background intensity. Image contrast refers to the measurement of the different brightness levels between the brightest white and the darkest black in the light and dark regions of an image. Achieving the highest image contrast is probably the most important factor when designing any machine vision system. Generally, the human eye requires a minimum contrast value of 0.02 to distinguish between an image and its background. For other detectors, such as cameras or CCD or CMOS devices, the minimum contrast is typically a different value. Improving image contrast is a necessary condition to achieve accurate image recognition. Modulating the spatial frequency of the microscopic image through optical filters to enhance contrast is one solution. An optical filter is a component intended to change the spectral intensity distribution or polarization state of electromagnetic radiation. The variation in the spectral intensity distribution may or may not depend on the wavelength. Optical filters may function via transmission, reflection, or in both manners. Optical filters function to alter the light within the optical imaging system. This can be used for observation purposes or to capture high-quality images with a camera. Each filter can serve a different purpose and filters can be used for various improvements, such as enhancing contrast, blocking ambient light, removing harmful UV or IR rays, selectively omitting or transmitting specific wavelengths of light (such as excitation light), correcting the light path problem, and reducing the intensity of the light.

Optical notch filters, commonly referred to as band-stop or reject filters, are designed to transmit most wavelengths with low-intensity loss while reducing the optical range within a specific wavelength to a very low level. Optical thin-film notch filters have the basic structure of optical interference filters. Notch filters can be applied to visual optics to improve image contrast. Recently, Sulejman et al. [1] presented the application of commercially available thin-film spectral notch filters to phase-contrast imaging of transparent samples. They demonstrated enhanced contrast imaging of wavefields introduced by spatial light modulators and unstained biological samples. Their results showed instantaneous phase-contrast imaging without post-processing, allowing direct imaging using a camera or the eye. In 2016, Hoggan et al. [2] proposed an optical notch filter with a wavelength centered at 480 nm to reduce direct stimulation of intrinsically photosensitive retinal ganglion cells. They developed two filters: the therapeutic filter blocked visible light at 480 nm and a 620 nm filter was designed as a sham intervention. These preliminary findings suggest that lenses equipped with thin-film optical notch filters may be helpful in the treatment of chronic migraines. Kim et al. [3] obtained spectral images with wavelengths of 750, 850, and 900 nm through optical filters, aiming to improve the contrast of old documents. Images or text can be enhanced through optical filters. In terms of non-invasive optical detection, these filters are widely used in food, fruit, and vegetable quality detection, and optical filters with appropriate characteristics are selected according to different color characteristics [4–8]. In the process of the microscopic inspection of thin-film surfaces, machine vision often uses a program algorithm to determine the surface defect area, with its robustness directly affecting the interpretation of the image, such that the machine vision can determine the result for the defect area due to the difference in pattern distribution. The difference is that the defect area cannot be objectively quantified in all images [9]. In 2019, Hyttinen et al. [10] reported a method that can be used to implement the positive and negative parts of optical filters separately and apply the effect from a partially negative optical filter for imaging purposes. The partially negative filters are split into positive and negative parts that can then be implemented optically. They demonstrated the method's feasibility with the examples of a color chart and dental imaging. In 2021, they also presented an enhancement of dental and oral feature visibility based on a portable spectral camera and computational filters derived from the analysis of the principal components. When computational filters are applied to oral and dental spectral images, selected features of clinical interest can be highlighted based on the surrounding environment [11].

To achieve an optical notch filter design, Zhang et al. [12] presented the design and production approach for an ultra-steep notch filter and demonstrated excellent correspondence with the theoretical spectral performance. They designed an ultra-steep notch filter with high transmittance (no back-side reflections included) in the wavelength ranges of 400–500 nm and 550–700 nm and high reflectivity in the spectral region from 500 to 550 nm. The notch filter can be produced with ion-assisted electron beam deposition technology with a high deposition rate and good stress quality. Lyngnes and Kraus [13] proposed an optimization method for discrete-layer notch filters. The apodized thickness-modulated design method was demonstrated to generate discrete-layer notch filter designs with very low ripple in the transmission regions and without the need for numerical optimization. A multilayer thin-film notch filter is also known as a rugate filter. Lappschies et al. [14] presented a binary digitized rugate filter fabricated using the ion beam sputtering technique. They designed a rugate notch filter for illumination technology applications. The transmitting regions of this filter ranged from 400 to 480 nm and from 655 nm to the near-IR spectral range. The rugate design for the multilayer filter comprised a sinusoidal modulation of the refractive index containing 17.5 periods superimposed with an additional symmetrical period of a negative cosine function. Li et al. [15] used the high/low refractive index of TiO_2 and Al_2O_3 to design a rugate notch filter at wavelengths of 510–590 nm with a total physical thickness of 1.2 μm. They modulated the refractive index and film thickness of Al_2O_3 and TiO_2 simultaneously using the atomic layer deposition (ALD) technique and adjusted the product of the refractive index and film thickness to fluctuate similarly to a wrinkle. ALD deposition technology can provide thin-film filters with very high step coverage. The authors successfully prepared a notch filter with a center wavelength of 550 nm and an average reflectivity of 86.7% at wavelengths from 510 to 590 nm.

In our previous publications, the multilayer design and fabrication of an optical notch filter were proposed with the aim of improving visual quality [16]. A nine-layer notch filter composed of SiO_2 and Nb_2O_5 thin films with a central wavelength of 480 nm was prepared using electron beam evaporation combined with ion-assisted deposition. We designed and manufactured the optical notch filter in order to see more detail by making it more visible against the background. In 2021, a lower-stress laser protective lens based on a multilayer notch filter was presented [17]. The transmission of the proposed notch filter was 0.2% at the central wavelength of 532 nm, and the average transmission of the transmission band was about 70%. In this work, among the three primary colors red, green, and blue, the colors of the optical notch filters were chosen to be red and blue for the design target. The two colors red and blue are complementary, and there is a strong contrast between the two colors. Therefore, the center wavelengths of the notch filters were designed to correspond to 480 and 620 nm for blue and red, respectively (hereafter referred to as 480 and 620 filters). Optical interference filters with multiple notch bands can be combined by stacking thin films with different notch-band designs. However, depositing the thin-film stacks on the same side of the glass substrate leads to the accumulation of greater residual stress on the notch filter. If the residual stress is too high, the surface of the thin film will peel or crack. In order to solve the problem of excessive residual stress, we propose a method involving depositing multilayer thin films on both sides of a substrate as residual stress compensation, which can reduce the stress value for the multilayer thin films.

To enhance the microscopic image contrast, a customized optical interference filter with two notch bands was developed by depositing thin films on both sides of the substrate. A dual-band notch filter with central wavelengths of 480 and 620 nm was deposited on both sides of a transparent glass substrate to compensate for residual stress. In other words, when using the same material and film thickness ratio, a single-wavelength 480 nm notch filter and a 620 nm notch filter have similar residual stress values. It was expected that the dual-wavelength notch filter would be able to effectively reduce residual stress and improve image contrast due to the double-sided coating on the same glass substrate.

2. Materials and Methods

2.1. Design of Optical Notch Filters

The optical notch filter was designed using Essential Macleod optical thin film software (Thin Film Center Inc., Tucson, AZ, USA.) [18]. The notch filter design consisted of alternating stacked layers of low-refractive-index SiO_2 thin film and high-refractive-index Ta_2O_5 thin film. We designed three kinds of optical multilayer notch filters with different central wavelengths and different transmittances: single-wavelength notch filters with central wavelengths of 480 and 620 nm and a dual-wavelength notch filter (480 and 620 nm dual-band). It was hoped that, through the simulation and analysis of the multilayer notch filter, the design and process parameters of the notch filter could be modified, providing a reference for manufacturing optical thin-film devices with special functions. This would be helpful to develop coating technology for optical notch filters based on a multilayer film structure.

The design specification for the 480 nm notch filter was that the transmittance of the wavelengths at 460–500 nm was below 50%, the transmittance of the center wavelength at 480 nm was below 20%, and the average transmittance of the other transmission bands was greater than 80%. The design specification for the single-wavelength 620 nm (red-light band) notch filter was that the transmittance of the wavelengths at 580–600 nm was below 50%, the transmittance of the center wavelength at 620 nm was below 20%, and the average transmittance of the other transmission bands was greater than 90%. The initial design of the multilayer thin-film structure was 6L(3H3L)^x, where H is a high-refractive-index thin film and L is a low-refractive-index thin film. After optimization of the thin-film stack, a value for x of at least 4 would meet the design requirements. After using Essential Macleod software to fine-tune and optimize the thickness of the thin film, the optimized design result was 6.02L(2.7H3.01L)^4, which met the requirements. Table 1 shows the multilayered structure designs for the single-wavelength 480 and 620 nm notch filters.

Table 1. The multilayer structure designs for the single-wavelength 480 and 620 nm notch filters.

Layer	Materials	Refractive Index	Film Thickness (nm)	
			480 nm Notch Filter	620 nm Notch Filter
1	SiO_2	1.460	243.76	317.07
2	Ta_2O_5	1.984	178.21	232.78
3	SiO_2	1.460	243.76	317.07
4	Ta_2O_5	1.984	178.21	232.78
5	SiO_2	1.460	243.76	317.07
6	Ta_2O_5	1.984	178.21	232.78
7	SiO_2	1.460	243.76	317.07
8	Ta_2O_5	1.984	178.21	232.78
9	SiO_2	1.460	487.52	634.13

2.2. Notch Filter Preparation

In the preparation of the thin films, three optical notch filters were prepared using a double electron gun evaporation system (Showa Shinku Co., Sayama-city, Saitama, Japan). The coating equipment was as follows: the vacuum system consisted of an oil rotary pump, a mechanical booster pump for rough evacuation, a diffusion pump for fine evacuation, and a helium cold trap to capture water vapor in the form of helium condensation in an air compressor to help improve the efficiency of the evacuation rate. The background pressure was 2.7×10^{-4} Pa. The working gases used in the process were argon (99.999%) and oxygen (99.999%). The maximum output power of the electron gun was 10 kW, the voltage was 10 kV, and the current was 1 A. The evaporation materials used in the process were all grain-like, with a particle size of about 1–3 mm and a purity of 99.99%. Before the deposition of the thin film, materials such as Ta_2O_5 were premelted with an electron beam with a power of 2.0 kW. The coating material was evaporated with an electron beam with a power of 3.0 kW. The deposition rate was 0.10 nm/s for Ta_2O_5 and 0.4 nm/s for SiO_2. The substrate was heated to 150 °C during the process. The anode current of the ion source for the ion-assisted deposition was 0.5–10 A, the anode voltage was 80–300 V, the ion energy was 50–200 eV, and the divergence angle was 60 degrees. Quartz and optical monitoring systems were adopted to monitor the thickness of the thin film. The quartz monitoring system used a 5 MHz quartz crystal oscillator. The optical monitoring system adopted a photospectrometer with a wavelength range of 360 to 1000 nm and measured the change in reflectivity when a thin film was deposited on the substrate by reflection. The extreme points of reflectivity were used for the stop-coating action, and the optical monitoring sheet was made of B270 glass material.

2.3. Characteristic Measurements of Optical Notch Filters

For the measurement of optical properties, a Shimadzu UV2600i (Shimadzu, Nakagyo Ku, Kyoto, Japan) was used to measure the transmittance of the notch filters, which had a wavelength range of 400 to 1000 nm. To study the effects of different notch filters on the image contrast, we added the proposed filters to the microscope with a magnification of 500 and evaluated the image contrast with a MATLAB-based software program. The contrast sensitivity was calculated using the following formula.

$$\text{Contrast} = \frac{\mathrm{I_{max}} - \mathrm{I_{min}}}{\mathrm{I_{max}} + \mathrm{I_{min}}} \quad (1)$$

where $\mathrm{I_{max}}$ is the maximum light intensity of the image and $\mathrm{I_{min}}$ is the minimum light intensity.

In this study, the thin film sample was observed with an optical microscope and a CMOS camera (model: Basler acA3088-57um), and three different notch filters were added to compare the contrast values. Figure 1a shows a schematic diagram of the measurement system used to evaluate image contrast. The working distance was 30 mm and the actual size of the test sample was 25 mm in diameter. A light source formed a parallel beam through a collimator. The beam splitter divided the light into two parallel beams, one of which was directed towards the test sample through a microscope objective and a notch filter. The light reflected by the test sample returned through the beam splitter and was directed to the CMOS camera, where an image was formed and displayed on a computer monitor.

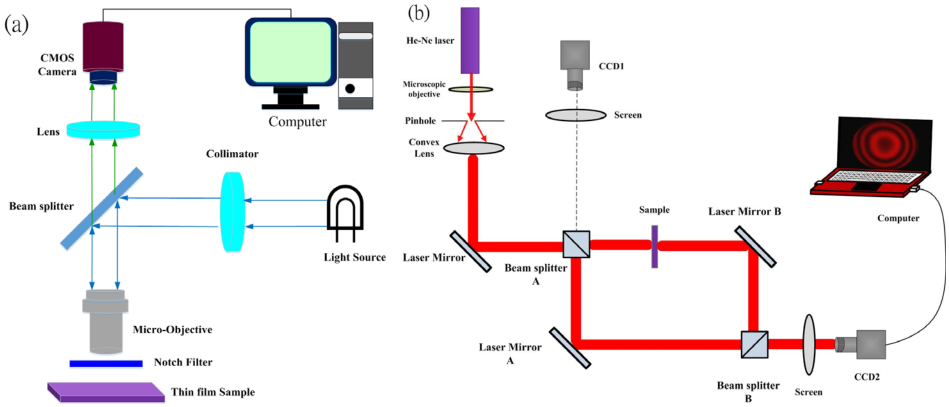

Figure 1. Schematic diagram of the measurement system for (**a**) evaluating image contrast and (**b**) measuring residual stress.

A Mach–Zehnder interferometer was used to measure the residual stress in the thin films, as shown in Figure 1b. The measuring system used a helium-neon laser (Melles Griot, Artisan Technology Group, Champaign, IL, USA) with a wavelength of 632.8 nm as the light source. The spatial filter was used to form a point light source, and then a uniform parallel beam was generated through a collimating lens. The incident beam was divided into two beams after passing through the first beam splitter. The beams passing through the second beam splitter were finally recombined into a single beam, which was imaged on a ground glass screen and formed an interference fringe. The CCD camera was used to capture the interference pattern, and the computer analyzed the image captured by the CCD camera. We developed a MATLAB program to process all interferograms. The surface profile of the optical thin film could be reconstructed using the fast Fourier transform method [19] and the phase-unwrapped method [20]. The radius of curvature of the thin-film samples could be determined with the curve fitting method. The residual stress in thin films is related to the change in the radius of curvature before and after film deposition. The residual stress value in thin films can be determined using the modified Stoney's formula [21,22].

$$\sigma = \frac{E_s \times t_s^2}{6(1 - v_s)t_f}\left(\frac{1}{R_2} - \frac{1}{R_1}\right) \quad (2)$$

where σ is the residual stress in the thin film, ν_s is the Poisson's ratio for the substrate, E_s is the Young's modulus for the substrate, t_f is the thickness of the film, t_s is the thickness of the substrate, and R_1 and R_2 represent the radius of curvature of the substrate before and after coating.

The fabricated notch filters were also subjected to microstructural inspection. The root-mean-square (RMS) surface roughness of the notch filters was measured with a Linnik microscopic interferometer, which has been described in previous publications [23,24]. In the Linnik microscopic interferometer, one beam is directed onto a test surface through a cube beam-splitter and a microscope objective (20×), while another beam is reflected by a reference mirror (flatness $\lambda/20$) and a cube beam-splitter. The resulting interference fringe pattern is recorded by a CCD camera. For the measurement range, 240 × 240 pixels can be chosen for analysis, indicating that the actual size is 100 × 100 μm.

Atomic force microscopy (AFM) is a powerful tool for measuring surface roughness at the nanometer scale. The tip of the atomic force microscope scans over the sample's surface to measure the topography. The tip interacts with the sample surface, and the forces between the tip and sample are recorded to create a topographic image of the sample's surface. The root-mean-square (RMS) roughness of thin films can be calculated by averaging the deviations in height from the mean surface height squared over the scanned area. This gives a measure of the average height variations on the sample surface. Scanning electron microscope (SEM) works by scanning a beam of high-energy electrons over the surface of a sample, which causes the electrons to interact with the atoms on the surface and produce signals that can be detected to create an image of the sample. In addition, the surface microstructure and cross-sectional images of the multilayer thin-film filters were observed using a cold-field emission scanning electron microscope (model: Hitachi FESEM S-4800, Tokyo, Japan). SEM can provide information about the topography and composition of thin films, as well as their morphology, crystal structure, and defects. SEM can also be used to analyze the thickness and uniformity of a thin film by measuring the intensity of the signals produced.

3. Results and Discussion

3.1. Optical Transmittance Measurement

To assess whether the multilayer notch filter met the design of the optical properties, the optical transmittance of the multilayered notch filter was measured. Figure 2a shows a notch filter with a center wavelength of 620 nm (that is, the 620 filter) deposited on the first surface of the glass substrate. The ripple of the passband was similar to the design spectrum, and the transmittance of the stopband at the center wavelength of 620 nm was 18.3%, which met the design specifications. Figure 2b shows a multilayer notch filter with a center wavelength of 480 nm coated on the second surface to form a dual-wavelength 620 and 480 nm notch filter. In the transmission spectrum, it can be seen that the transmittance of the multilayer thin film with a central wavelength of 620 nm was maintained at 18.3%, and the transmittance of the multilayer thin film with a central wavelength of 480 nm was 14.6%. The ripple distribution of the passband was also consistent with the design. In order to evaluate the optical properties of the center wavelength 480 nm notch filter, a 480 nm notch filter deposited on one side of the substrate was also prepared as a control sample. This research involved the design and fabrication of optical notch filters with different center wavelengths of 480 and 620 nm to enhance image contrast. For example, a double-sided coating technique was adopted for the dual-wavelength (480 and 620 nm) notch filter to reduce residual stress. The first side was coated with a nine-layer notch filter with a central wavelength of 480 nm, and the second side was coated with a nine-layer notch filter with a central wavelength of 620 nm. The transmission spectrum of the multilayered notch filter with dual wavelengths of 480 and 620 nm is shown in Figure 2c. The transmittance of the stop band was about 15%. Compared to the single-wavelength notch filter, the transmittance difference may have been affected by the reflection of the uncoated surface, and the transmission band ripple distribution of the 480 nm notch filter was also consistent with the design.

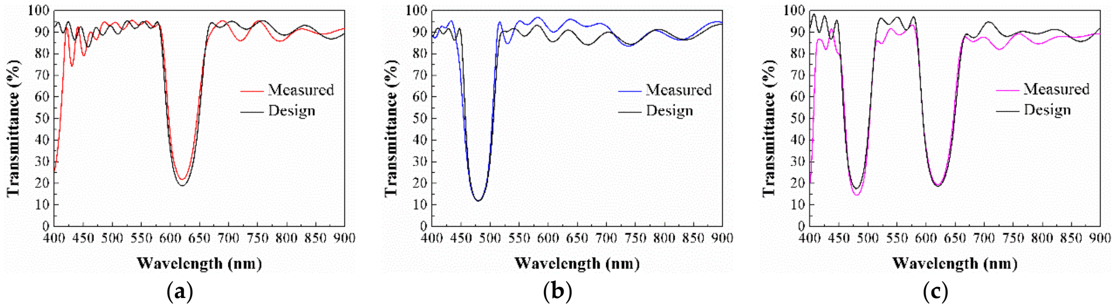

Figure 2. Transmission spectra for different notch filters: (**a**) 480 nm filter; (**b**) 620 nm filter; (**c**) 620 and 480 nm filter.

We considered the effect of changing the incident angle of light on the transmittance of the notch filters. Figure 3 shows the change in transmittance for the test filters as the angle of incidence was increased from 0° to 50° with intervals of 10°. The center wavelength of the 620 nm notch filter (coated on the front surface) shifted from 621 to 551 nm. With the increase in the incident angle, the center wavelength transmittance of the stopband increased from 18.3% to 23.3%. The ripple in the passband was similar to the design of the 620 nm notch filter, as shown in Figure 3a. In a similar manner, the optical transmittance of the single-wavelength 480 nm notch filter was measured at different incident angles, and the results showed that the center wavelength of the 480 nm notch filter used as the control sample shifted from 480 to 427 nm. When the incident angle increased to 50°, the central wavelength transmittance of the stopband increased from 14.6% to 19.8%, as shown in Figure 3b. Due to the 620 nm notch filter deposited on the first side, the wavelength shift in both notch bands could be observed simultaneously. The results showed that the combination of single-wavelength 480 and 620 nm notch filters formed a dual-wavelength notch filter, and the overall center wavelength shift was small. It is worth noting that the ripple in the passband of the dual-wavelength (480 and 620 nm) notch filters at different incident angles was different from that of single-sided coated notch filters. The larger the incident angle was, the greater the difference. When the incident angle was 50°, it was observed that the transmittance dropped to 75% at wavelengths between 600 nm and 625 nm, as shown in Figure 3c. This was because the optical path difference between the reflected light waves in the two sets of the film stack structures decreased when the light waves were obliquely incident on the double-side coated notch filter. The reflection bands of the two film stacks shifted to short wavelengths simultaneously. It also affected the ripple in the transmission band.

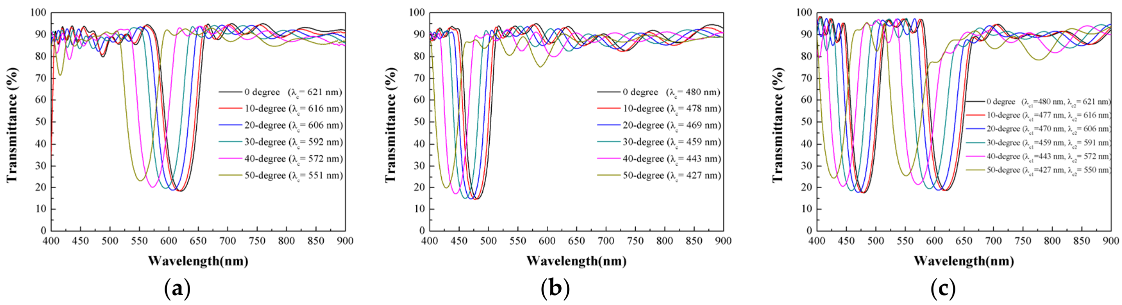

Figure 3. Transmission spectra for notch filters at different incident angles: (**a**) 620 nm filter; (**b**) 480 nm filter; (**c**) 620 and 480 nm filter.

Figure 4 shows photographs of three kinds of optical notch filter. The color of the 620 nm multilayer notch filter on the glass was light blue (cyan), as shown in Figure 4a. Figure 4b shows the appearance of a single-sided coating with a 480 nm multilayered notch filter, which was yellow in color. The 480 nm multilayered notch filter was deposited on the second side of the B270 glass to form a dual-wavelength notch filter and the color turned dark green, as shown in Figure 4c. When viewed at an oblique angle, the optical properties of the notch filters showed various colors as a result of the change in the optical path difference.

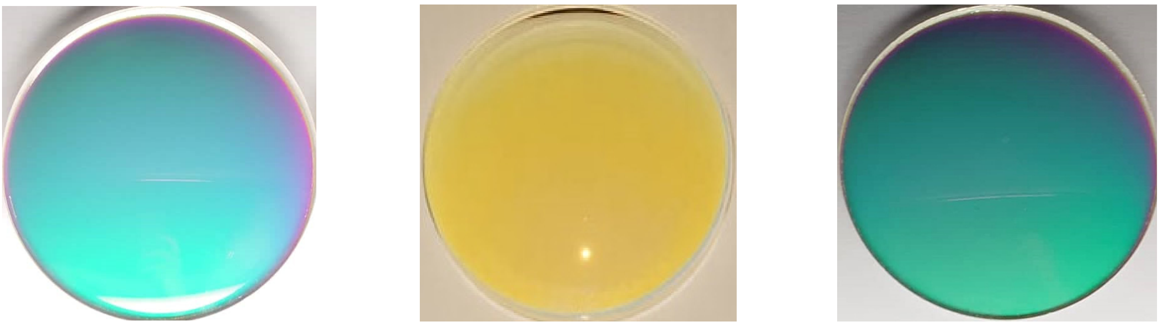

(**a**) (**b**) (**c**)

Figure 4. Photographs of different notch filters: (**a**) 620 nm filter; (**b**) 480 nm filter; (**c**) dual-wavelength 620 and 480 nm filter.

Different notch filters were used to compare the image contrast, and three notch filters with 480, 620 nm, and dual wavelengths were added to the optical microscope for image observation. It was seen from the optical microscope that the thin-film sample appeared as severely deformed with cracks. In order to see the cracks more clearly, an optical microscope with a magnification of 500 was used for observation and image capture, and then a MATLAB-based program was used for image processing to calculate the image contrast. The contrast values for the three different notch filters were evaluated, as shown in Figure 5. The contrast without the notch filter was about 0.328. When using the 480 nm notch filter to observe the sample, the contrast was 0.545, which was higher than that without the notch filter. Black cracks and defects could be observed. When the sample was viewed with a 620 nm notch filter, the contrast was 0.470, which was lower than with a 480 nm notch filter. When we used a dual-wavelength 480 and 620 nm notch filter, we could obtain a clearer image, including seeing more grains and cracks, and the contrast value was 0.696, which was better than the first two notch filters. It can also be seen from the transmission spectrum in Figure 2 that the single-wavelength 480 and 620 nm notch filters could reduce the intensity of blue and red light, respectively. These two colors corresponded to the dark and bright features in the microscope image. From the experimental results, it can be seen that there were more bright areas than dark areas. When using a 620 nm notch filter, the improvement in contrast was not better than that with a 480 nm notch filter. Figure 5 shows that the contrast value without using the notch filter was 0.328, and after adding the 480, 620 nm, and 480 and 620 nm notch filters, the contrast values increased to 0.545, 0.470, and 0.696, respectively. In this work, the experimental results showed that all three notch filters could improve the contrast of microscopic images.

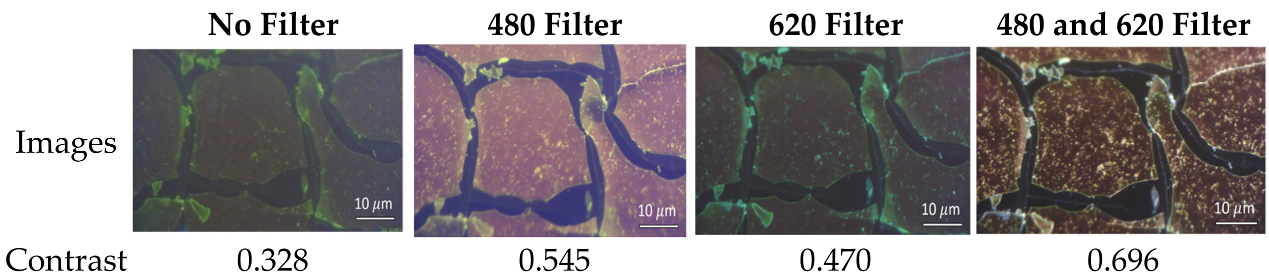

Figure 5. Contrast values for three notch filters for microscope image observation.

3.2. Residual Stress Measurement in Thin Films

Residual stress is the main threat to the durability of thin-film interference filters, so it is necessary to measure and predict the residual stress in optical thin-film filters [25,26]. However, there is currently no generally applicable theory for the prediction of residual stress in thin films. Therefore, device designers usually do not have sufficient information on residual stress values when designing thin-film devices [27]. In this study, the residual stress in a single-sided coated notch filter was evaluated using a Twyman–Green interferometer [16,17] and the residual stress in a double-sided coated notch filter was measured using a Mach–Zehnder interferometer. To evaluate the effect of double-sided thin-film coating on residual stress compensation, a 620 nm filter was deposited on the first surface of the B270 glass and a 480 nm filter was deposited on the second surface of the B270 glass. The surface deformation and the radius of curvature changes in the film/substrate were measured, and the residual stress was calculated from the Stoney formula. Figure 6 shows the 3D surface contour of the bare substrate and the multilayered 620 nm notch filter. The 3D surface profile of the bare substrate was concave and its P-V (peak–valley) value was 0.422 µm. For the 620 nm notch filter, the first surface of the substrate was coated with a 620 nm notch filter and the 3D surface profile formed a convex surface with a P-V value of approximately 0.368 µm. Figure 7 shows the 3D surface contour of the substrate without coating and with the 480 nm notch filter after deposition. The 3D surface profile of the bare substrate was concave and its P-V value was 0.194 µm. For a 480 nm notch filter, the 3D surface profile formed a convex surface with a P-V value of approximately 0.626 µm. Figure 8 shows the surface profile of the substrate without coating and with the 480 and 620 nm notch filter after deposition. The 3D surface contour of the bare substrate was concave and its P-V value was 0.368 µm. After depositing a dual-band notch filter, the 3D surface profile formed a concave surface with a P-V value of approximately 0.391 µm. The above results indicate that there were significant changes in the contour and P-V values of the substrate after multilayer thin film deposition, and residual stress evolution was also exhibited during the thin-film coating process.

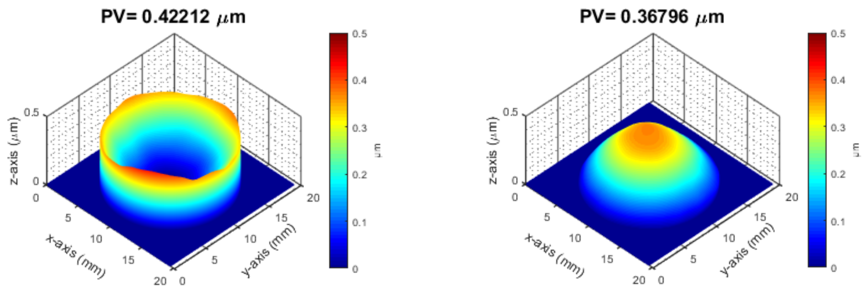

(**a**) (**b**)

Figure 6. Three-dimensional (3D) surface contour of the substrate (**a**) without coating and (**b**) with 620 nm notch filter deposition.

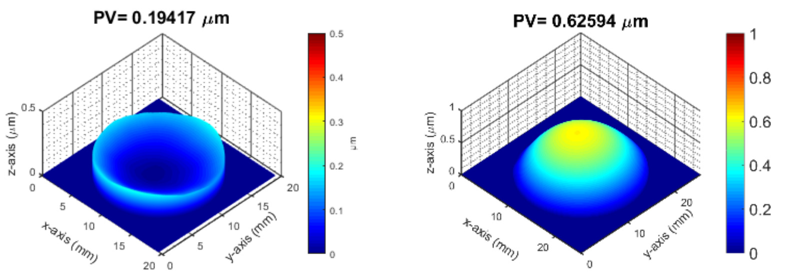

(**a**) (**b**)

Figure 7. Three-dimensional (3D) surface contour of the substrate (**a**) without coating and (**b**) with 480 nm notch filter deposition.

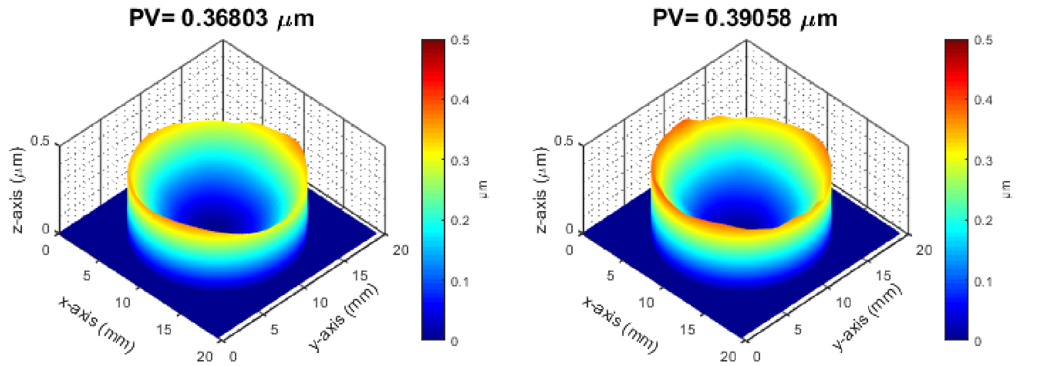

(**a**) (**b**)

Figure 8. Three-dimensional (3D) surface contour of the substrate (**a**) without coating and (**b**) with 480 and 620 nm notch filter deposition.

Different thin-film materials and process technologies can affect the residual stress and deformation in the thin film, and they must be determined using measurement experiments. The curvature radii were 297.5 m for the bare substrate, −86.2 m for the 480 nm notch filter, and −80.5 m for the 620 nm notch filter, respectively. The residual compressive stress in the single-sided coating was −256 MPa for the 480 nm filter and −217 MPa for the 620 nm filter. Furthermore, the radius of curvature before coating was 91.96 m and the radius of curvature after double-sided coating was 81.50 m. Thus, the residual tensile stress in the double-sided 480 and 620 nm filter was 10.8 MPa. It can be seen that the stress compensation effect could be achieved after the multilayer notch filter was deposited on both sides, effectively reducing the residual stress in the thin film. If the glass substrate is subjected to compressive stress, the surface profile may change from concave to convex. In this work, the use of double-sided coating technology to reduce residual stress in multilayer interference filters was consistent with the findings from other studies [28]. In other related work, Begou et al. [28] successfully deposited bandpass filters with two wavelength ranges on double-sided glass. After accounting for the deformation of the thin film and the substrate due to the residual stress induced by the deposition of the multilayer film on one side, the filter was passed through. Multilayer thin films were deposited on the back side of the substrate to offset some of the residual stress. They reduced the bandpass filter to -16.73 ± 3 nm on a 24 mm × 26 mm substrate. The authors pointed out that double-sided deposition can be used not only to reduce residual stress but also to superimpose the properties of two filter stacks, allowing a single component to have dual-wavelength high-transmission or reflection bands.

3.3. Microstructural Characteristics Measurements

Surface roughness is one of the important characteristics of precision optical components. If the surface roughness is too high, it will cause a serious loss affecting the optical component and reduce the transmittance of the passband. Therefore, it was necessary to measure the surface roughness of the multilayer notch filter. Figure 9 shows the root-mean-square (RMS) surface roughness measurements for different notch filters obtained using a Linnik microscopic interferometer. The surface roughness values were 2.09 ± 0.11 nm for the 480 nm filter and 1.80 ± 0.11 nm for the 620 nm filter, respectively. The experimental results show that the two types of notch filters had lower surface roughness and lower scattering loss, which may have resulted in higher transmittance in the passband. We also used atomic force microscopy (AFM) to measure the RMS surface roughness of single-side coating notch filters. Figure 10 shows that the surface roughness values were 2.216 nm for the 480 nm filter and 1.807 nm for the 620 nm filter, respectively. The surface roughness values of the multilayer notch filter were measured using a Linnik microscopic interferometer and AFM, both of which gave similar values, as indicated by the results.

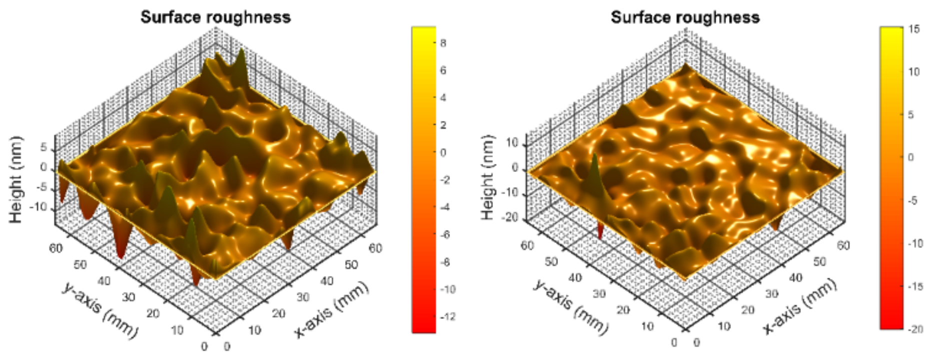

(**a**) (**b**)

Figure 9. Surface roughness of the notch filters measured with a Linnik microscopic interferometer: (**a**) 480 nm filter and (**b**) 620 nm filter.

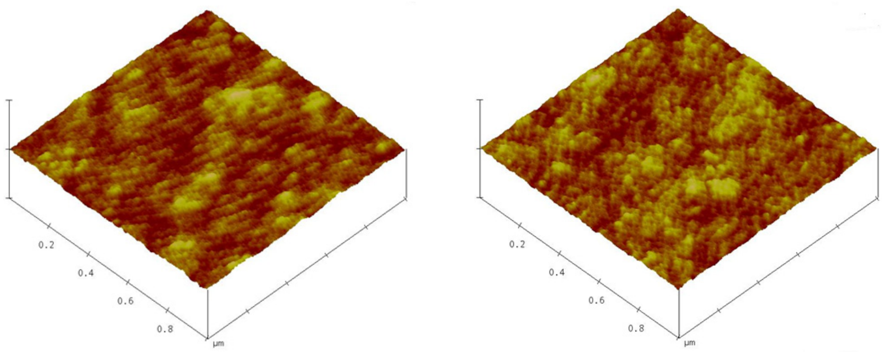

(**a**) (**b**)

Figure 10. Surface roughness of the notch filters measured with atomic force microscopy: (**a**) 480 nm filter and (**b**) 620 nm filter.

The packing density of a multilayer film structure can be qualitatively observed through microstructure analysis, and the packing density of a multilayer film structure is closely related to the residual stress. Therefore, the influence of the residual stress on the film structure can be determined through microstructure analysis. Figures 11a and 12a show the SEM images of the top view of the microstructures of the 620 and 480 nm notch filters, respectively. The difference between the two notch filters was small, the grains were fine, and the surface was smooth. Figures 11b and 12b show cross-section views of the 620 and 480 nm notch filters. The columnar structure and the number of layers can be seen in the cross-section view. The SEM images clearly show each layer, with the black interface being a SiO_2 thin film and the gray interface being a Ta_2O_5 thin film. It can be seen that the microstructure of the thin film was mostly continuous and dense, and the thin film had a columnar structure.

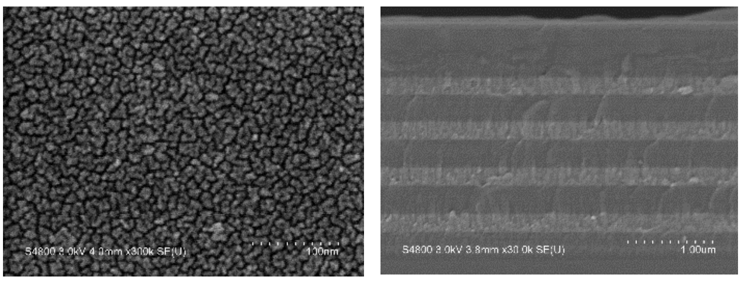

(**a**) (**b**)

Figure 11. FE-SEM image of 620 nm filter: (**a**) top view and(**b**) cross-section.

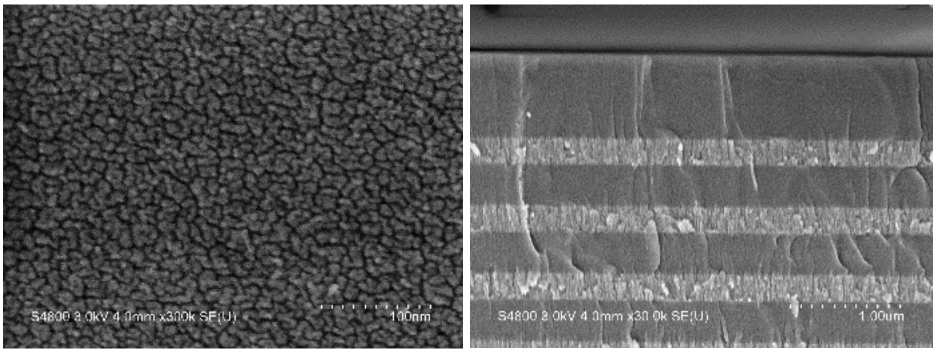

(**a**) (**b**)

Figure 12. FE-SEM image of 480 nm filter: (**a**) top view and (**b**) cross-section.

4. Conclusions

In this study, two single-wavelength notch filters and one dual-wavelength notch filter (620 and 480 nm) were prepared using an electron-beam evaporation with IAD technique. For the optical properties, the transmittances of the notch filters at the center wavelengths of 480 and 620 nm with normal incidence were 17.5% and 18.5%, respectively. The results from the microscope observation significantly improved the clarity and contrast of the thin-film image. We added 620 and 480 nm notch filters in front of the thin film sample with an optical microscope to obtain higher contrast images. For the residual stress in the notch filter, after depositing a 480 nm notch filter on the back surface of the 620 nm notch filter, the residual stress decreased from −256 to 10.8 MPa. The surface contour of the substrate changed from convex to concave, indicating a transition from compressive stress to small tensile stress. The residual stress in the dual-band (wavelengths of 480 and 620 nm) notch filter could be reduced using a double-sided coating technique. The residual stress in the dual-band notch filter was much lower than that in the single-wavelength notch filters, which is beneficial for machine vision applications and reliable durability. In the surface roughness measurements, the RMS surface roughness was measured by AFM, which showed values of 2.216 for the 480 nm notch filter and 1.807 for the 620 nm notch filter. This indicated that it had low scattering loss characteristics and could maintain high transmittance in the passband. In the FE-SEM microscopic image, it can be seen that the particles on the surface of the notch filter were fine and smooth. In the side view of the structure, the structure of the SiO_2 film was mostly continuous and dense, while the Ta_2O_5 film was observed as a columnar structure. Using the proposed notch filters, the results observed with an optical microscope significantly improved the clarity and image contrast. The results also indicated that the optical properties of the dual-band notch filter were superior to those of single-wavelength notch filters, improving the contrast of the image observation. In summary, the proposed optical notch filters can provide rich and saturated colors with good stability while also providing durable, low-residual-stress performance in terms of mechanical properties. They have potential applications in machine vision, biological imaging, and dynamic monitoring.

Author Contributions: Conceptualization, C.-L.T.; methodology, C.-L.T. and S.-H.S.; writing—review and editing, C.-L.T.; validation, C.-L.T. and S.-H.S.; formal analysis, C.-L.T. and C.-Y.C.; data curation, Y.-M.C. and D.-H.M. All authors have read and agreed to the published version of the manuscript.

Funding: The authors are grateful for the financial support from the Taiwan Ministry of Education for this research project. This research was supported in part by the National Science and Technology of Council under project No. MOST 111-2622-E-035-003. This study was also supported by Feng Chia University (contract No. 21H00723).

Institutional Review Board Statement: Not applicable.

Informed Consent Statement: Not applicable.

Data Availability Statement: Not applicable.

Acknowledgments: The authors are grateful to the Precision Instrument Support Center of Feng Chia University for providing AFM and SEM analytical facilities.

Conflicts of Interest: The authors declare no conflict of interest.

References

1. Sulejman, S.B.; Priscilla, N.; Wesemann, L.; Lee, W.S.L.; Lou, J.; Hinde, E.; Davis, T.J.; Roberts, A. Thin film notch filters as platforms for biological image processing. *Sci. Rep.* **2023**, *13*, 1–9. [CrossRef] [PubMed]
2. Hoggan, R.N.; Subhash, A.; Blair, S.; Digre, K.B.; Baggaley, S.K.; Gordon, J.; Brennan, K.C.; Warner, J.E.A.; Crum, A.V.; Katz, B.J. Thin-film optical notch filter spectacle coatis for the treatment of migraine and photophobia. *J. Clin. Neurosci.* **2016**, *28*, 71–76. [CrossRef] [PubMed]
3. Kim, S.J.; Deng, F.; Brown, M.S. Visual enhancement of old documents with hyperspectral imaging. *Pattern Recognit.* **2011**, *44*, 1461–1469. [CrossRef]
4. Cubero, S.; Aleixos, N.; Moltó, E.; Gómez-Sanchis, J.; Blasco, J. Advances in Machine Vision Applications for Automatic Inspection and Quality Evaluation of Fruits and Vegetables. *Food Bioprocess Technol.* **2010**, *4*, 487–504. [CrossRef]
5. ElMasry, G.M.; Nakauchi, S. Image analysis operations applied to hyperspectral images for non-invasive sensing of food quality—A comprehensive review. *Biosyst. Eng.* **2016**, *142*, 53–82. [CrossRef]
6. Al-Mallahi, A.; Kataoka, T.; Okamoto, H.; Shibata, Y. Detection of potato tubers using an ultraviolet imaging-based machine vision system. *Biosyst. Eng.* **2009**, *105*, 257–265. [CrossRef]
7. Ariana, D.; Guyer, D.E.; Shrestha, B. Integrating multispectral reflectance and fluorescence imaging for defect detection on apples. *Comput. Electron. Agric.* **2006**, *50*, 148–161. [CrossRef]
8. Abdullah, M.; Mohamad-Saleh, J.; Fathinul-Syahir, A.; Mohd-Azemi, B. Discrimination and classification of fresh-cut starfruits (*Averrhoa carambola* L.) using automated machine vision system. *J. Food Eng.* **2006**, *76*, 506–523. [CrossRef]
9. Cartwright, S.L.; Kenkel, J.G. Optical Filtering for Machine Vision Applications. In *Optics, Illumination, and Image Sensing for Machine Vision*; SPIE: Bellingham, WA, USA, 1987; Volume 728, pp. 266–271. [CrossRef]
10. Hyttinen, J.; Fält, P.; Jäsberg, H.; Kullaa, A.; Hauta-Kasari, M. Optical implementation of partially negative filters using a spectrally tunable light source, and its application to contrast enhanced oral and dental imaging. *Opt. Express* **2019**, *27*, 34022–34037. [CrossRef]
11. Hyttinen, J.; Falt, P.; Jasberg, H.; Kullaa, A.; Hauta-Kasari, M. Computational Filters for Dental and Oral Lesion Visualization in Spectral Images. *IEEE Access* **2021**, *9*, 145148–145160. [CrossRef]
12. Zhang, J.; Tikhonravov, A.V.; Trubetskov, M.K.; Liu, Y.; Cheng, X.; Wang, Z. Design and fabrication of ultra-steep notch filters. *Opt. Express* **2013**, *21*, 21523–21529. [CrossRef] [PubMed]
13. Lyngnes, O.; Kraus, J. Design of optical notch filters using apodized thickness modulation. *Appl. Opt.* **2013**, *53*, A21–A26. [CrossRef] [PubMed]
14. Lappschies, M.; Görtz, B.; Ristau, D. Application of optical broadband monitoring to quasi-rugate filters by ion-beam sputtering. *Appl. Opt.* **2006**, *45*, 1502–1506. [CrossRef] [PubMed]
15. Li, Y.; Shen, W.; Hao, X.; Lang, T.; Jin, S.; Liu, X. Rugate notch filter fabricated by atomic layer deposition. *Appl. Opt.* **2014**, *53*, A270–A275. [CrossRef]
16. Tien, C.-L.; Lin, H.-Y.; Cheng, K.-S.; Chiang, C.-Y.; Cheng, C.-Y. Design and Fabrication of a Cost-Effective Optical Notch Filter for Improving Visual Quality. *Coatings* **2021**, *12*, 19. [CrossRef]
17. Tien, C.L.; Lin, H.Y.; Cheng, K.-S.; Chang, C.-K. Design and fabrication of laser protective lenses based on multilayered notch filter with low residual stress and low surface roughness. *Coatings* **2021**, *11*, 1513. [CrossRef]
18. MacLeod, H.A. *Thin-Film Optical Filters*, 4th ed.; CRC Press: Boca Raton, FL, USA, 2010.
19. Takeda, M.; Ina, H.; Kobayashi, S. Fourier-transform method of fringe-pattern analysis for computer-based topography and interferometer. *Appl. Opt.* **1982**, *72*, 156–160.
20. Macy, W.W., Jr. Two-dimensional fringe-pattern analysis. *Appl. Opt.* **1983**, *22*, 3898–3901. [CrossRef]
21. Stoney, G.G. The tension of metallic films deposited by electrolysis. *Proc. R. Soc. Lond. Ser. A Math. Phys. Sci.* **1909**, *82*, 172–175. [CrossRef]
22. Tien, C.-L.; Zeng, H.-D. Measuring residual stress of anisotropic thin film by fast Fourier transform. *Opt. Express* **2010**, *18*, 16594–16600. [CrossRef]
23. Tien, C.-L.; Yang, H.-M.; Liu, M.-C. The measurement of surface roughness of optical thin films based on fast Fourier transform. *Thin Solid Films* **2009**, *517*, 5110–5115. [CrossRef]
24. Tien, C.-L.; Yu, K.-C.; Tsai, T.-Y.; Lin, C.-S.; Li, C.-Y. Measurement of surface roughness of thin films by a hybrid interference microscope with different phase algorithms. *Appl. Opt.* **2014**, *53*, H213–H219. [CrossRef] [PubMed]
25. Tien, C.-L.; Lin, H.-Y. Accurate prediction of multilayered residual stress in fabricating a mid-infrared long-wave pass filter with interfacial stress measurements. *Opt. Express* **2020**, *28*, 36994–37003. [CrossRef] [PubMed]
26. Tien, C.-L.; Chen, K.-P.; Lin, H.-Y. Internal Stress Prediction and Measurement of Mid-Infrared Multilayer Thin Films. *Materials* **2021**, *14*, 1101. [CrossRef] [PubMed]

27. Huff, M. Review Paper: Residual Stresses in Deposited Thin-Film Material Layers for Micro- and Nano-Systems Manufacturing. *Micromachines* **2022**, *13*, 2084. [CrossRef]
28. Begou, T.; LeMarchand, F.; Lemarquis, F.; Moreau, A.; Lumeau, J. High-performance thin-film optical filters with stress compensation. *J. Opt. Soc. Am. A* **2019**, *36*, C113–C121. [CrossRef]